Hot electron injection: An efficacious approach to charge LaCoO₃ for improving the water splitting efficiency

Bo-Tao Zhang [a,1], Jun Liu [a,b,1], Shizhong Yue [b], Yanguo Teng [a], Zhijie Wang [b,*], Xiaobao Li [c,*], Shengchun Qu [b,d,**], Zhanguo Wang [b]

[a] College of Water Sciences, Beijing Normal University, Beijing 100875, China
[b] Key Laboratory of Semiconductor Materials Science, Beijing Key Laboratory of Low Dimensional Semiconductor Materials and Devices, Institute of Semiconductors, Chinese Academy of Sciences, Beijing, 100083, China
[c] School of Civil Engineering, Hefei University of Technology, Hefei 230009, China
[d] College of Materials Science and Opto-Electronic Technology, University of Chinese Academy of Sciences, Beijing 100049, China

ARTICLE INFO

ABSTRACT

In order to acquire an efficient photo-catalyst for generating hydrogen directly on the material, herein, we introduce the well-known catalyst, LaCoO₃, to the community of water splitting using solar energy. By combining with Au nanoparticles, we find that hot electrons injected from Au nanoparticles to LaCoO₃ are responsible for amplifying the photo-catalytic efficiency and the well-known thermal-stimulus for driving chemical transformations is not observed to be influential. Such charging process to the catalysts is crucial for promoting the subsequent catalytic reactions. Thus, this paper provides insights into the working mechanism of plasmonic based photo-catalyst.

© 2017 Elsevier B.V. All rights reserved.

1. Introduction

The design of cost-effective and high-efficient photo-catalyst for solar energy conversion is crucial in the world-wide pursuit of sustainable energy, with extensive efforts being undertaken [1,2]. As the efficacious catalysts for electrochemical water splitting, ABO₃-based pervoskite oxides have been proven to be of high promises. The specific oxygen vacancies and the occupancy of electron orbital for surface transition metal ions are responsible for the high efficiency [3]. In the system of electrochemical water splitting, charge carriers (electrons/holes) for initiating the reactions are from the external circuit and a power supply element is required. To get rid of it and make the system self-powered, it is of feasibility to use solar energy to drive the reactions. These oxides, however, are either with a large band gap that is not appropriate for solar energy absorption, or with a band structure that needs more investigations [4–6].

Owning to the effect of surface plasmons resonance (SPR), the coherent oscillations of electrons in nano-metals that can be stimulated by a wide range of electromagnetic waves, metallic nanostructures are attractive components to amplify the photo-electrochemical reactions in combination with the conventional photo-catalysts [7–9]. The excited energy transfer from the nano-metals that could improve the absorption efficiency of the adjacent semiconductors, the hot charge injection to the semiconductor and the enhanced local electric field are responsible for the performance improvement [10,11]. Even without these semiconductors, metallic nanostructures alone also present impressive capability in photo oxidation of organic molecules. Thermal and photonic stimuli are demonstrated to be effective in driving chemical transformations [12].

Herein, we aim to introduce the well-known electrochemical catalyst, LaCoO₃, to the photo-electrochemical solar energy conversion. Both of the experiment and simulation aspects demonstrate that the corresponding material has a band gap of 1.39 eV, which is suitable for solar energy absorption. A p-type semiconductor feature of the as-grown material is concluded. By forming hybrid structure with Au nanoparticles, the composite nanostructure presents a decent improvement in photo-electrochemical

hydrogen generation. The charge injection from the excited Au nanoparticles to $LaCoO_3$ contributes to such performance improvement.

2. Experimental

2.1. Preparation of $LaCoO_3$ photo-catalysts and $LaCoO_3/Au$ hybrid photo-catalysts

$LaCoO_3$ nanoparticles were prepared through the sol-gel method. Briefly, a certain amount of lanthanum nitrate, cobalt nitrate and citric acid were respectively weighed at the stoichiometric ratio of 1:1:2. Lanthanum nitrate and cobalt nitrate were added to 10 mL ethylene glycol monomethyl ether solvent, and placed in a magnetic stirrer with constantly stirring. When it was completely dissolved, the citric acid was slowly added to the mixture. After stirring for 2 h, the mixture was allowed to stand for 24 h. After all, a $LaCoO_3$ precursor solution was obtained. The concentration of lanthanum ion in the precursor solution was 0.2 mol/L. The solution was evaporated and heated to dry on a magnetic hot plate. The amorphous powder was then calcined at 800 °C for 2 h with the heating rate of 5 °C/min in a muffle furnace to obtain the final $LaCoO_3$ nanoparticles.

The $LaCoO_3/Au$ hybrid photo-catalysts were fabricated in two steps: the synthesis of Au nanoparticles and the loading of it on $LaCoO_3$ by calcination. The synthesis of Au nanoparticles was carried out using the method of sodium citrate reduction as the literature reported [13]. For 0.5%wt. Au nanoparticles, 0.125 mL $HAuCl_4 \cdot 4H_2O$ solution (20 mg/mL) was diluted to 50 mL. The above solution was then heated to boiling point, and a certain amount of Na_3-citrate (1%wt.) was added as the mass ratio to $HAuCl_4 \cdot 4H_2O$ of 1:1. Then 0.239 g $LaCoO_3$ was weighed and added to the above solution. The mixture was evaporated and heated to dry with constantly stirring on a magnetic hot plate to obtain the mixture of Au nanoparticles and $LaCoO_3$ nanoparticles. Then the mixture was calcined at 500 °C for 2 h with the heating rate of 5 °C/min in a muffle furnace to obtain the $LaCoO_3/Au$ hybrid photo-catalysts.

2.2. Characterizations of catalyst

The crystalline phase was identified by X-ray diffraction (XRD) measurements taken with Cu K_α radiation (X pert pro MPD) in the 2-theta range of 20°–80°. The morphology characterization of the $LaCoO_3/Au$ hybrid photo-catalysts and Au nanoparticles was carried out in a high resolution transmission electron microscopy (HRTEM) of a Tecnai G2 F30 S-TWIN. Surface electronic states were analyzed by X-ray photoelectron spectroscopy (XPS, ESCSLAB 250Xi) with Al $K\alpha$ radiation. The UV–vis spectra were recorded on TU1950 spectrophotometer. Steady-state Photoluminescence (PL) spectrum was measured at room temperature on Cary Eclipse Fluorescence (Varian) with an excitation wavelength of 605 nm. The time-resolved photoluminescence (TRPL) spectra were obtained on Edinburgh Analytical Instruments F900 with a resolution of 100 ps. The position of energy levels for $LaCoO_3$ was achieved by ultraviolet photoemission spectroscopy (UPS, Axis Ultra DLD).

2.3. Photo-catalytic H_2 production and reaction mechanism analysis

The photo-catalytic reaction was evaluated in an online photocatalytic H_2 production system (Labsolar-III (AG), Perfectlight, Beijing) equipped with a GC2014 (Shimadzu). The photo-catalyst ($LaCoO_3$ or $LaCoO_3$-Au hybrid photo-catalysts, 0.1 g) was suspended in aqueous formaldehyde solution (100 mL, 37%–40%) with a magnetic stirrer. The system was evacuated to remove the air present in the reaction mixture. Irradiation was conducted by a

500 W xenon lamp and the irradiation intensity was monitored by a radiation meter (Thorlabs, PM100D with S310C). The reaction temperature was controlled by a low-constant temperature bath (DC-2006, Shanghai Bilang). The evolved hydrogen was gathered and analyzed by GC (TCD and FID, molecular sieve 5 Å column and Ar carrier). The other gaseous productions were also detected by GC and the liquid productions were detected by HPLC (LC-20A, Shimadzu, C18 column, 5% flow of acetonitrile and 95% flow of phosphoric acid solution with 0.02% concentration).

Computational details and *photo-electrochemical characterization* are given in the Supplementary Information.

3. Results and discussion

Both $LaCoO_3$ powder and thin film were synthesized via a convenient sol-gel approach. Fig. 1a shows the XRD pattern of the as-grown material. The series of diffraction peaks matches well with the standard pattern of $LaCoO_3$ (PDF#84-0848). In particular, the peaks at 32.858°, 33.225° and 47.463° are attributed to diffraction of (-1,1,0) (1,1,2) and (2,2,0) crystal planes, respectively. The crystal structure is depicted as the inset in Fig. 1a. XPS spectra of the material are given in Fig. 1b–d. The La 3d peaks with shake-up features located at 830–840 eV and 850–857 eV are characteristic of La(III) [14]. In Co 2P spectrum, the peaks at 778.3 and 793.7 eV are the typical characteristic of Co(III) with the typical shake-up structure at 789.92 eV [15]. The O 1s spectrum presents two mains peaks: the one at 528.87 eV is attributed to the perovskite oxygen whereas the one at 531.37 eV is from the oxygen in hydroxides or carbonates [14]. To be more important, theses oxygen sites at the surface are crucial for the catalytic reactions.

To get more convincing information on semiconductor nature of the material, band gap structure was calculated by DFT (density functional theory) simulation using the crystal structure revealed by the XRD pattern. As shown in Fig. 2a, a band gap structure of 1.39 eV is demonstrated. Fig. S1 shows the absorption spectrum of the material, and the resulting Tauc plot demonstrates a band gap value of 1.39 eV for the as-grown $LaCoO_3$. The photoluminescence spectrum is given in Fig. S2 and an outstanding peak at 826 nm, attributing to the band edge emission, could be observed. Such band gap value is suitable for absorbing solar energy and enables the material as a good candidate in photo-electrochemistry.

Photo-electrochemical measurements of the photoelectrodes based on $LaCoO_3$ film were performed in a 0.1 M KCl aqueous solution. A Pt counter electrode and Ag/AgCl reference electrode were used during the measurements. Under chopped illumination, the electrode showed a standard cathodic photocurrent, indicative of a typical p-type feature of the material (Fig. 2b). The according Mott-Schottky plot is shown in Fig. 2c and the p-type feature could also be concluded. The plot yields a flat band potential of 1.42 eV vs Ag/AgCl. Detailed information for the analysis is given in the Supplementary Information. These results indicate that we have provided a promising p-type semiconductor to hydrogen generation. The relative narrow band gap structure and the oxide stability make the material advantageous over the conventional p-type semiconductors, like Si, GaP, Cu_2O and NiO [16–20].

In order to use the material for hydrogen generation in a high efficiency, we combine it with Au nanoparticles. The size of Au nanoparticles is characterized around 50 nm by the TEM image in Fig. S3 and the clear crystal lattices imply a high crystal quality of it. Fig. S4 displays the absorption spectrum of Au nanoparticles, and the absorption in the visible range is from the coherent oscillations of electrons excited by the photons, particularly the photons with the wavelength at 530 nm. These portions of light absorption could be used to drive catalytic reactions by forming the composite nanostructures.
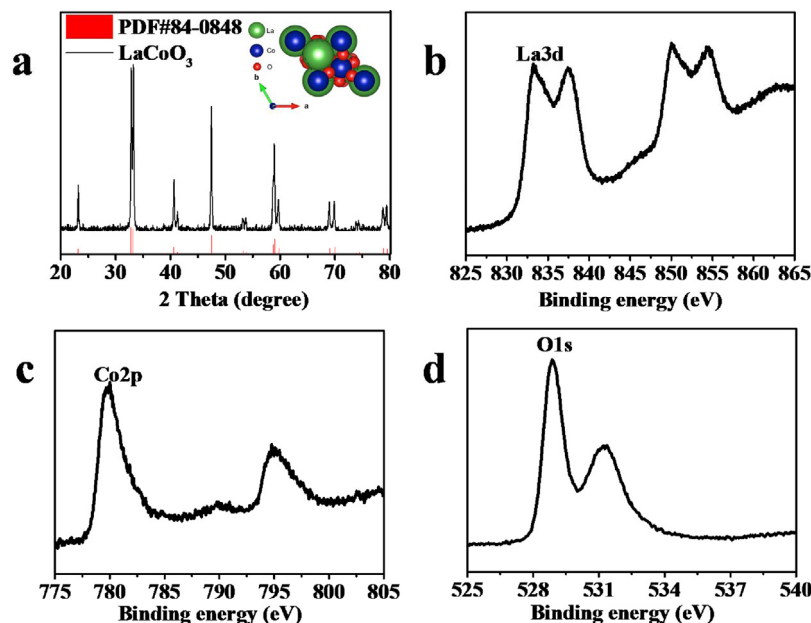
Fig. 1. (a) XRD pattern and (b-d) XPS spectra of $LaCoO_3$ nanoparticles synthesized at 800 °C by the sol-gel method.
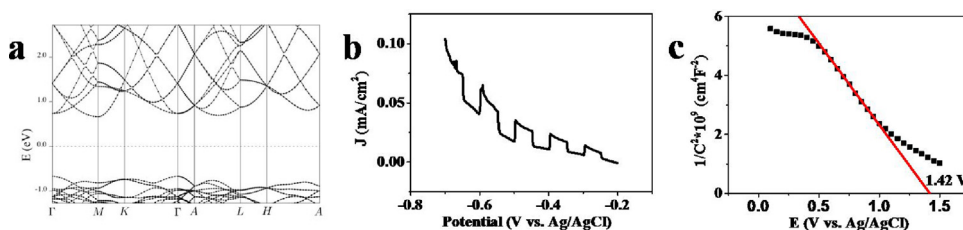

Fig. 2. (a) Band gap structure calculated by the DFT simulation. (b) Linear sweep voltammograms under chopped illumination. (c) Mott-Schottky characteristic.
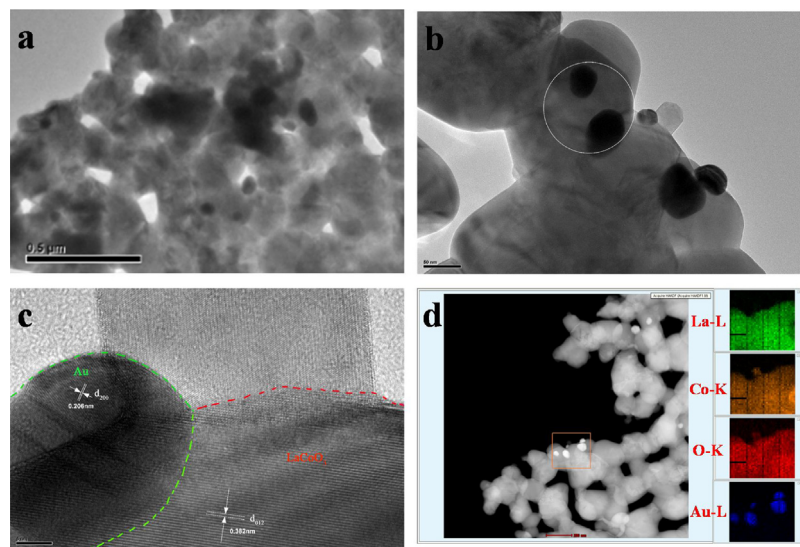

Fig. 3. TEM images (a, b), HRTEM image (c) and HAADF-STEM image (d) of $LaCoO_3$/Au nano-composite.

The procedure for combining the two materials was performed by dispersing $LaCoO_3$ particles in the aqueous solution with Au nanoparticles. After removing the solvent by evaporation, the resultant was annealed at 500 °C for 2 h. Fig. 3a and b shows the TEM images of the $LaCoO_3$/Au composite in different resolutions. The size of the $LaCoO_3$ is gauged in the range of 200–500 nm, while the size of Au nanoparticles keeps constant. More resolved TEM image is shown in Fig. 3c, where the crystal lattices of both Au and $LaCoO_3$ could be clearly discerned. Importantly, the two materials present a good quality of contact, thus favorable for the charge transfer between them. To delineate the combination and spatial distribution of $LaCoO_3$ and Au, the HAADF-STEM measurement was employed. From the pictures with distinct color contrast in Fig. 3d, the La, Co, O and Au elemental maps could be observed, which
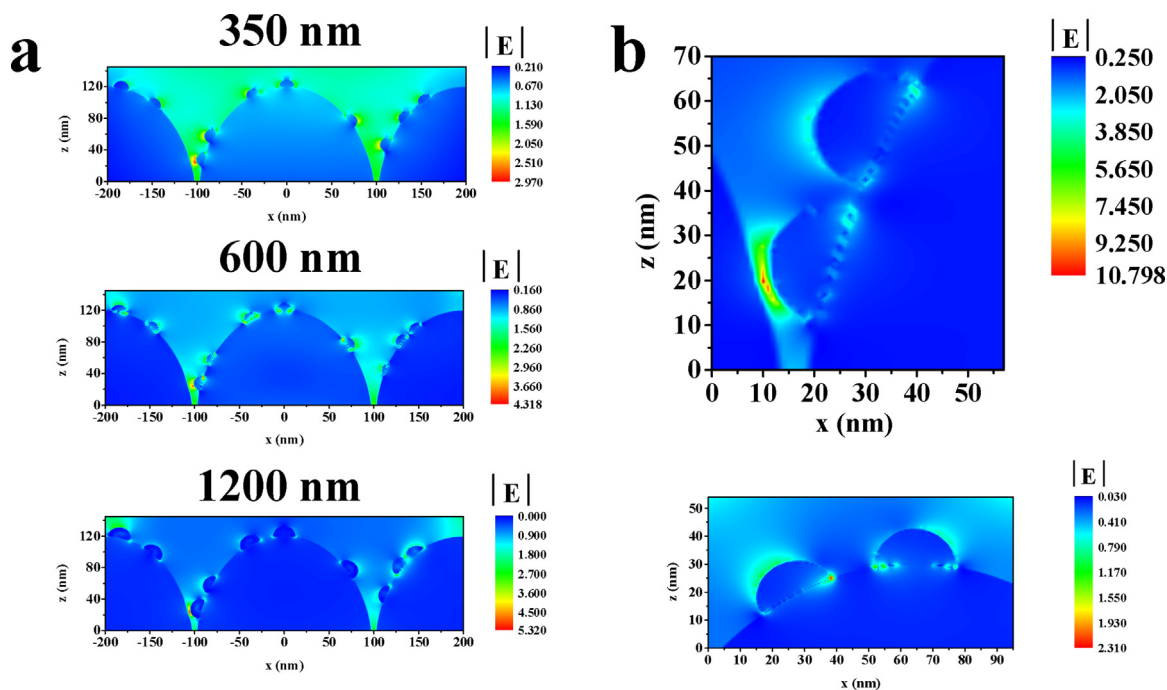
Fig. 4. Electric field simulated by FDTD solutions at 350 nm, 600 nm and 1200 nm illuminations in a large scale (a) and at 600 nm illumination in a small area (b).

illustrate that LaCoO$_3$ and Au nanoparticles are closely contacted with each other. To further confirm the chemical composition of the prepared LaCoO$_3$/Au composite, energy-dispersive X-ray (EDX) measurement was carried out in the area selected in Fig. 3b and the relevant results are shown in Fig. S5, where we could definitely get the signals from La, Co, O and Au.

Fig. S6 presents the absorption spectrum of the composite nano-structure. Though the content of Au nanoparticles is controlled as low as 2%wt. and the spectra of the two components overlap in the visible region, the presence of Au nanoparticles could indeed improve the absorption efficiency of the system. The well-known surface plasmonic effect of the Au nanoparticles is responsible to the improvement. This effect could also result in a large localized electric field at the surface of Au. As shown in Fig. 4a and b, we have simulated the electric field using FDTD (finite-different time-domain) solutions. Under the illuminations at 350 nm, 600 nm, and even 1200 nm, respectively, the structure shows a series of hot spots at the surface of Au and the interface of Au and LaCoO$_3$. Such hot spots in the electric field could promote the catalytic reactions by charging the adjacent LaCoO$_3$.

Hydrogen generation measurements were carried out by dispersing the photo-catalytic powders in the aqueous solution with formaldehyde as sacrificial hole acceptor under a white illumination with a power density of 300 mW/cm^2. Fig. 5a presents the hydrogen evolution of the LaCoO$_3$ loading with different amounts of Au nanoparticles. In comparison with the bare sample, the composite structures show an obvious enhancement in hydrogen generation. The optimized amount of 0.5%wt. Au in LaCoO$_3$ results in the highest hydrogen generation efficiency, 42 μmol h^{-1} g^{-1}. Less amount of Au has a limited SPR effect for performance improvement and overload of Au would reduce the absorption efficiency of LaCoO$_3$ and the contact area of LaCoO$_3$ with the electrolyte.

The dependence of the hydrogen generation rate on the reaction temperature is given in Fig. 5b. The photo-catalytic system containing LaCoO$_3$ nanoparticles shows an interesting feature of hydrogen generation rate vs temperature. With the temperature increasing from 0 to 15 °C, the rate increases sharply. As we then increase the temperature to 30 °C, however, the rate drops. This observation is not consistent with the conventional hydrogen generation kinetics, where the rate increases exponentially with $-1/T$ (T: temperature) [21]. Generally, the increasing temperature would make formalde-hyde and proton more active and these reactants are easier to bond to the active sites on the surface of LaCoO$_3$ and participate in the reactions with a low energy barrier. In this case, the increase in temperature is helpful for hydrogen generation in this system. A loss of photo-generated charge carriers for driving the water splitting reactions should be responsible for the deterioration of hydrogen generation rate at high temperature region. The loss was possibly caused by the nonradiative, multiphonon recombination of photogenerated charge carriers [22]. Therefore, these conflicting mechanisms impact the efficiency of hydrogen generation and the temperature of 15 °C is the point where the two mechanisms are in balance. Further enhancement in temperature would make the charge recombination mechanism become dominant. With respect to the system containing LaCoO$_3$/Au nano-composite, the rate of it is always higher than that without Au nanoparticles thus indicates that the presence of Au nanoparticles could promote the reactions of hydrogen generation. The trend of hydrogen generation rate vs temperature is similar to that in the system without Au nanoparticles. This phenomenon is not in agreement with the photo-catalytic case using plasmonic nanostructure only, where photo-catalytic quantum efficiencies on plasmonic metallic nanostructures increase with light intensity and operating temperature. The plasmonic nanostructures could effectively couple thermal and photonic stimuli to drive chemical transformations [12]. The only explanation for this observation is that the hydrogen generation reactions do not occur on the surface of Au nanoparticles but on the surface of LaCoO$_3$. A hot charge transfer from excited Au to LaCoO$_3$ is responsible for the hydrogen generation improvement.

To get more information on the reactions, dependence of hydrogen generation rate on the incident light intensity is given in Fig. 5c. When the light intensity is lower than 200 mW/cm^2, the two systems present nearly the same hydrogen generation rate and the rate of the LaCoO$_3$/Au system is even slightly lower than that of the LaCoO$_3$. The presence of Au nanoparticles does not improve the
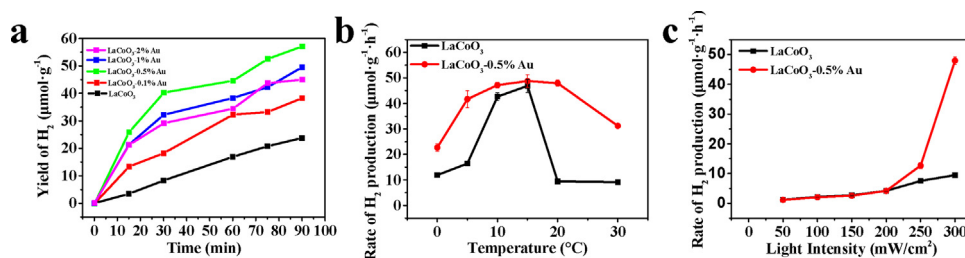
Fig. 5. (a) The hydrogen evolution of the $LaCoO_3$ loading with different amounts of Au nanoparticles. The reaction temperature was 5 °C and the irradiation intensity was 300 mW/cm^2. (b) The dependence of the hydrogen generation rate on the reaction temperature. The irradiation intensity was kept on 300 mW/cm^2. (c) The dependence of the hydrogen generation rate on the incident light intensity. The reaction temperature was kept at 20 °C.
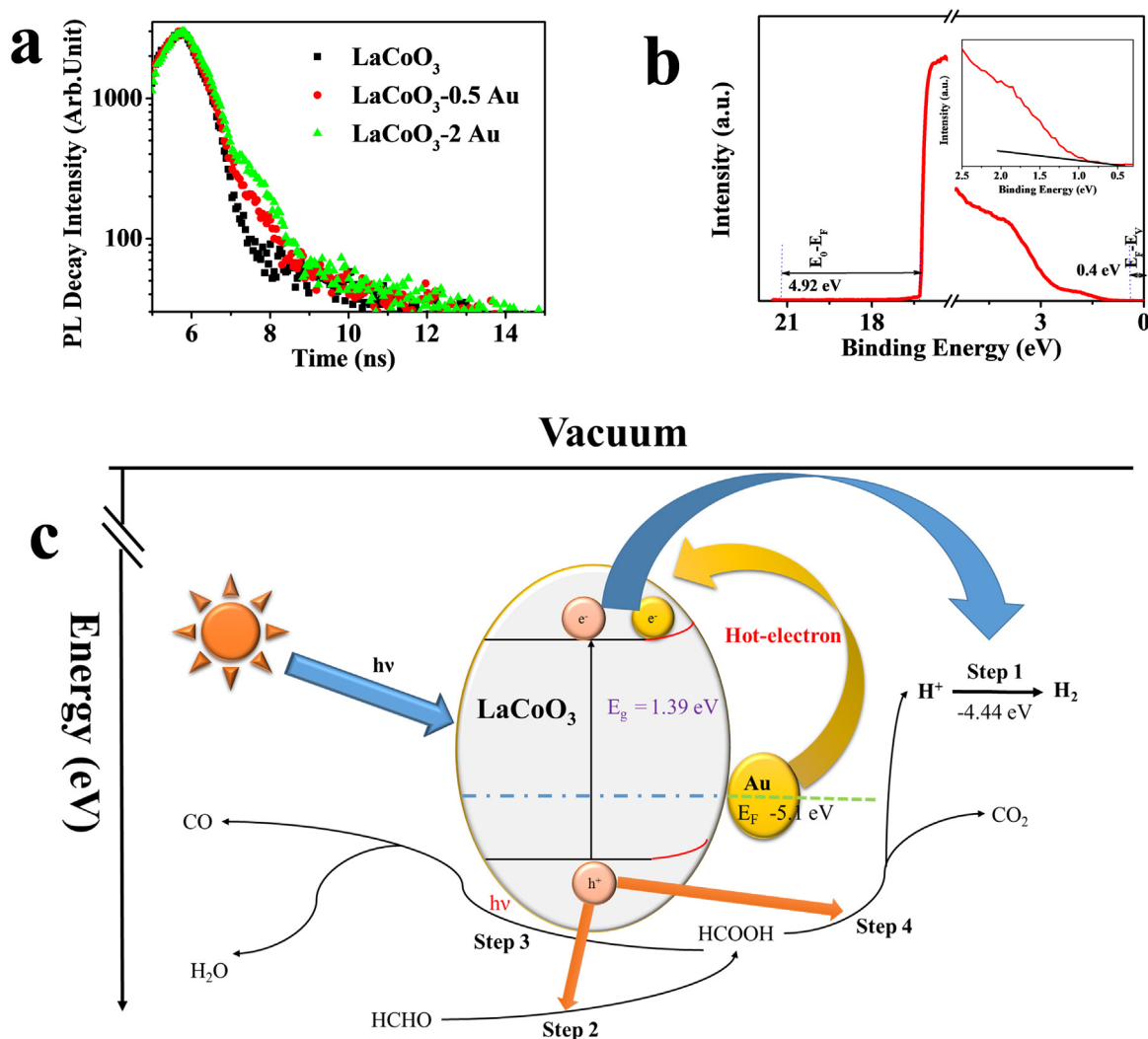
Fig. 6. (a) Emission decay profile for $LaCoO_3$, $LaCoO_3$-0.5 Au, $LaCoO_3$-2 Au. The excitation and monitored wavelength are 660 nm and 820 nm, respectively. (b) The direct UPS spectrum of bare $LaCoO_3$. (c) Scheme for the mechanism on the photo-generated charge transfer and catalytic reactions of the fabricated $LaCoO_3$/Au nano-composite.

photo-catalytic performance but deteriorates it slightly. The reason could be that the photon absorbed by Au nanoparticles could not be converted to active charge carriers to drive the photo-catalytic reactions when the light intensity is low. Surface plasmons, formed by the optical excitation of Au nanoparticles, relax by generating energetic hot electrons. These electrons could be either transferred to the surface of Au with electrolyte or injected to $LaCoO_3$ for driving the hydrogen generation reactions. Due to the stability of the Au surface where the active sites for hydrogen generation could be ignorable in comparison with the sites on $LaCoO_3$, only the elec-
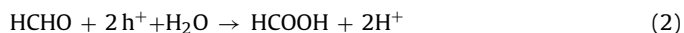
trons injected to $LaCoO_3$ could contribute to the photo-catalytic reactions. However, the hot electrons in Au nanoparticles need to overcome the barrier at the heterojuction of Au/$LaCoO_3$ to $LaCoO_3$. At low light intensity region, the generated hot electrons may not be energetic enough to transfer to $LaCoO_3$ for driving the reactions. As we tune the light intensity higher than 200 mW/cm^2, the system containing $LaCoO_3$/Au begins to deliver a higher hydrogen generation rate, in comparison with that without Au. A higher intensity results in a larger performance discrepancy. This indicates that the hot electrons generated by the light with high intensity could gain

enough active energy to pass over the barrier to LaCoO$_3$ and participate the catalytic reactions. The highly energetic hot electrons could be generated by the probability for excitation of electrons that are already vibrationally excited from previous electron scattering events [12,23].

To monitor the hot charge injection kinetics, transient photoluminescence measurements on LaCoO$_3$ and LaCoO$_3$/Au were performed by excitation at 660 nm. Fig. 6a shows that the addition of Au nanoparticles to LaCoO$_3$ could obviously enhance the lifetime of the photoluminescence signals. Using the standard single-exponential model, the lifetime was fit as 0.308 ns, 0.413 ns and 0.488 ns for the samples of LaCoO$_3$, LaCoO$_3$/0.5%wt. Au and LaCoO$_3$/2%wt. Au, respectively. These results demonstrate that the hot charge injection does occur and the density of electrons at the conduction band of LaCoO$_3$ has been increased accordingly.

Fig. 6b presents the UPS (ultraviolet photoemission spectroscopy) spectrum of the bare LaCoO$_3$, where the work function is measured as 4.92 eV and the valence band position vs the vacuum energy level is obtained as 5.32 eV. In addition to the band gap value calculated from the absorption spectrum, the band structure is acquired and depicted in Fig. 6c, where a standard p type feature could be concluded. Since water reduction level (E$_{red}$) is 4.44 eV with respect to E$_{vac}$, it shows that the conduction band (E$_{CB}$) of LaCoO$_3$ lies in the region of hydrogen generation. This demonstrates that LaCoO$_3$ is a good candidate for water reduction. Considering the 5.2 eV work function of Au, a Schottky barrier could be formed and the downward band bending from the Au to LaCoO$_3$ is favorable for collecting the hot electrons in excited Au nanoparticles and transferring them to the surface of LaCoO$_3$. However, the hot electrons have to be of high energy to pass over the Schottky barrier before being collected by LaCoO$_3$. This is consistent with the observation in Fig. 5c. Generally, the Schottky contact is key to the injection of hot electrons in Au to the adjacent semiconductors. For highly energetic hot electrons in Au, the downward band bending is kinetically favorable for the injection. For the hot electrons with a low energy, the injection is not preferential, due to the energy barrier. This case is of similarity to the case in Au/TiO$_2$ and Au/ZnO systems, where the hot electron injection is responsible for the impressive improvement in solar energy conversion [7,8,24].

The electrons at the excited state of LaCoO$_3$ initiate the water splitting reactions and release hydrogen by following the Reaction (1). To naturalize the holes in LaCoO$_3$, we used a standard pollutant, HCHO (formaldehyde), as the hole acceptor. In this case, we could decompose the pollutant and generate clear fuels synchronously. As demonstrated by Reaction (2), HCHO would get the excited holes and transform to HCOOH (formic acid), which could be decomposed under the light illumination to CO and H$_2$O (Reaction (3)). Using the analyses of both gas chromatography and liquid chromatography, we did observe the existence of H$_2$, CO and HCOOH in the reacting solution, as shown in Fig. S7. In addition, it is also of possibility that the HCOOH would be oxidized further to CO$_2$ by the holes as shown in Reaction (4). The relevant reaction kinetics are depicted in Fig. 6c. To expand the application of LaCoO$_3$ in water splitting, we also tried other sacrificial hole acceptors, including triethanolamine, diethanolamine and the mixture of Na$_2$S with Na$_2$SO$_3$. Obvious hydrogen generation could also be observed, as shown in Fig. S8.

$$2H^+ + 2e^- \rightarrow H_2 \tag{1}$$

$$HCHO + 2h^+ + H_2O \rightarrow HCOOH + 2H^+ \tag{2}$$

$$HCOOH + h\nu \rightarrow CO + H_2O \tag{3}$$

$$HCOOH + 2h^+ \rightarrow CO_2 + 2H^+ \tag{4}$$

Herein, we demonstrate that, for the photo-catalyst/plasmonic nanostructure, hot electrons generated in plasmonic metals are preferential to inject into the photo-catalyst to initiate the photo-electrochemical reactions, rather than staying on the metal surface for the reactions. The Schottky junction at the interface makes it energetically favorable for the hot electrons injecting to the photo-catalyst (semiconductors) before decaying in the metals [9,24]. The lifetime of initially generated hot electrons on metal surface is usually in the range of several picoseconds [25], while the lifetime of excited electrons in photo-catalysts is in the range of several nanoseconds as indicated by the transient PL (photoluminescence) spectra. Such difference results in the priority of the occurrence for the reactions on the photo-catalyst. More importantly, the photo-catalyst could also provide extensive active sites for the reactions. Thus, the LaCoO$_3$/Au system presents obvious two features of the photo-electrochemical reactions. First, the contour similarity about the curve of hydrogen generation rate vs temperature, for the systems of both LaCoO$_3$ and LaCoO$_3$/Au, indicates that the photo-electrochemical reactions occur on the surface of LaCoO$_3$. This feature is typical for the photo-catalytic reactions on the oxide semiconductors while the reactions on the surface of plasmonic nanostructures present a stark increase feature of hydrogen generation rate with the increase of temperature [25]. Second, the system of LaCoO$_3$/Au presents a superlinear dependence of hydrogen generation rate on incident light intensity while LaCoO$_3$ system exhibits lower rates as the incident light intensity increased. The superlinear feature is unique for the systems based on plasmonic nanostructures [25] and indicates that hot electrons generated in the plasmonic nanostructures indeed participate the photo-catalytic reactions on LaCoO$_3$ by injecting to the conduction band of LaCoO$_3$.

4. Conclusion

In summary, our results demonstrate that hot electron injection is a feasible approach to charge the photo-catalyst and enhance the according hydrogen generation rate. The reactions occur on the surface of LaCoO$_3$ and thermal stimuli are not helpful for the performance improvement but induce extra recombination of excited charge carriers at high temperatures. Insights on hot electrons generated in LaCoO$_3$/Au nano-composite for driving water splitting and HCHO decomposition reactions are thus provided in this work.

Appendix A. Supplementary data

Supplementary data associated with this article can be found, in the online version, at http://dx.doi.org/10.1016/j.apcatb.2017.07.033.

References

[1] H. Park, H. Kim, G. Moon, W. Choi, Energy Environ. Sci. 9 (2015) 411–433.
[2] M. Woodhouse, B.A. Parkinson, Chem. Soc. Rev. 38 (2008) 197–210.
[3] J. Suntivich, K.J. May, H.A. Gasteiger, J.B. Goodenough, Y. Shaohorn, Science 43 (2012) 1383–1385.
[4] W. Wang, M.O. Tade, Z. Shao, Chem. Soc. Rev. 44 (2015) 5371–5408.
[5] I. Bretos, R. Jiménez, D. Pérez-Mezcua, N. Salazar, J. Ricote, M.L. Calzada, Adv. Mater. 27 (2015) 2608.

[6] D. Meziani, A. Reziga, G. Rekhila, B. Bellal, M. Trari, Energy Convers. Manage. 82 (2014) 244–249.
[7] Z. Zhan, F. Grote, Z. Wang, R. Xu, Y. Lei, Adv. Energy Mater. 5 (2015) 1501654.
[8] Y. Mi, L. Wen, R. Xu, Z. Wang, D. Cao, Y. Fang, Y. Lei, Adv. Energy Mater. 6 (2015) 1501496.
[9] Z. Wang, D. Cao, L. Wen, X. Rui, M. Obergfell, M. Yan, Z. Zhan, N. Nasori, J. Demsar, L. Yong, Nat. Commun. 7 (2016) 10348.
[10] S. Linic, P. Christopher, D.B. Ingram, Nat. Mater. 10 (2011) 911–921.
[11] C. Clavero, Nat. Photonics 8 (2014) 95–103.
[12] P. Christopher, H. Xin, A. Marimuthu, S. Linic, Nat. Mater. 11 (2012) 1044–1050.
[13] G. Frens, Controlled Nucleation for the Regulation of the Particle Size in Monodisperse Gold Suspensions, Macmillan company, 1936.
[14] A. Glisenti, M. Pacella, M. Guiotto, M.M. Natile, P. Canu, Appl. Catal. B Environ. 180 (2016) 94–105.
[15] J.P. Dacquin, C. Lancelot, C.D. Dujardin, P. Costa, G. Djega-Mariadassou, P. Beaunier, S. Kaliaguine, S. Vaudreuil, S. Royer, P. Granger, Appl. Catal. B Environ. 91 (2009) 596–604.
[16] M. Chitambar, Z. Wang, Y. Liu, A. Rockett, S. Maldonado, J. Am. Chem. Soc. 134 (2012) 10670–10681.
[17] Z. Wang, A. Shakya, J. Gu, S. Lian, S. Maldonado, J. Am. Chem. Soc. 135 (2013) 9275–9278.
[18] D. Cao, N. Nasori, Z. Wang, L. Wen, R. Xu, Y. Mi, Y. Lei, Appl. Catal. B Environ. 198 (2016) 398–403.
[19] F.F. Abdi, Nat. Commun. 4 (2013) 2195.
[20] T.K. Townsend, N.D. Browning, F.E. Osterloh, Acs Nano 6 (2012) 7420.
[21] S.U. Jeong, R.K. Kim, E.A. Cho, H.J. Kim, S.W. Nam, I.H. Oh, S.A. Hong, S.H. Kim, J. Power Sources 144 (2005) 129–134.
[22] T.A. Westrich, K.A. Dahlberg, M. Kaviany, J.W. Schwank, J. Phys. Chem. C 115 (2011) 16537–16543.
[23] W. Ho, J. Phys. Chem. 100 (1996) 13050–13060.
[24] X. Zhang, Y. Liu, Z. Kang, Acs Appl. Mat. Interfaces 6 (2014) 4480–4489.
[25] M.L. Brongersma, N.J. Halas, P. Nordlander, Nat. Nanotechnol. 10 (2015) 25.